



Supported by



## Accepted Article

**Title:** The hydrodeoxygenation of glycerol over NiMoS<sub>x</sub>: catalyst stability and activity at hydrolysis conditions

**Authors:** Anthony D. Anderson, Michael P. Lanci, J. Scott Buchanan, James A. Dumesic, and George W. Huber

This manuscript has been accepted after peer review and appears as an Accepted Article online prior to editing, proofing, and formal publication of the final Version of Record (VoR). This work is currently citable by using the Digital Object Identifier (DOI) given below. The VoR will be published online in Early View as soon as possible and may be different to this Accepted Article as a result of editing. Readers should obtain the VoR from the journal website shown below when it is published to ensure accuracy of information. The authors are responsible for the content of this Accepted Article.

**To be cited as:** *ChemCatChem* 10.1002/cctc.202001289

**Link to VoR:** <https://doi.org/10.1002/cctc.202001289>

**Title:** The hydrodeoxygenation of glycerol over NiMoS<sub>x</sub>: catalyst stability and activity at hydrolysis conditions

**Author:** Anthony D. Anderson<sup>a</sup>, Dr. Michael P. Lanci<sup>b</sup>, Dr. J. Scott Buchanan, Prof. James A. Dumesic<sup>a</sup>, and Prof. George W. Huber<sup>a</sup>.

<sup>a</sup> Department of Chemical and Biological Engineering, University of Wisconsin, 1415 Engineering Drive, Madison, Wisconsin 53706, United States

<sup>b</sup> ExxonMobil Research and Engineering, 1545 Route 22 East Annandale, New Jersey 08801, United States

**Target journal:** ChemCatChem

**Corresponding author:** Prof. George W. Huber, gwhuber@wisc.edu

Accepted Manuscript

**Abstract:**

Catalytic activity tests were run to elucidate the chemistry and catalyst stability for the hydrodeoxygenation of glycerol and other aliphatic oxygenates over a NiMoS<sub>x</sub>/Al<sub>2</sub>O<sub>3</sub> catalyst at different pretreatments at hydrolysis conditions in a continuous flow reactor. Reactivity metrics were developed to quantify and compare the reactivity of NiMo for deoxygenation, hydrogenation, and C-C cleavage. Activity experiments showed sulfided NiMo and reduced NiMo catalysts had similar deoxygenation and hydrogenation activity for glycerol HDO at 400°C and 270 psig H<sub>2</sub> with the NiMoS<sub>x</sub> catalyst showing higher C-C cleavage activity. Without a sulfur co-feed, both the NiMoS<sub>x</sub> and NiMoO<sub>x</sub> catalysts lost >40% deoxygenation activity over 30 h time on stream. With a 2100 ppm H<sub>2</sub>S co-feed the NiMoS<sub>x</sub> catalyst showed a 12 times decrease in the deactivation rate for deoxygenation and 6 time decrease in the deactivation rate for hydrogenation. The main products at high conversion were propylene, propane, ethylene, methane, CO, methanol, ethanol, and 1-propanol. At low conversion, the major products were unsaturated allyl alcohol, acrolein, hydroxyacetone, and acetaldehyde. With no H<sub>2</sub>S co-feed at short contact times, there was a significant amount of carbon loss possibly due to condensation reactions, while at 2100 ppm H<sub>2</sub>S in the feed, the carbon balance was 102.4%. Temperature programmed oxidation of the spent NiMoS<sub>x</sub> catalysts after 30 h of glycerol HDO without an H<sub>2</sub>S co-feed showed that one of the causes of deactivation was coking.

## 1. Introduction:

Fast pyrolysis of lignocellulose is a process in which woody biomass is rapidly heated and thermally depolymerized to form bio-oil. Efficient utilization of the bio-oil is challenging as the poor fuel characteristics such as low-energy density (16-22MJ/kg), high water content, and high acidity ( $\text{pH} < 3$ ) hinder its use in most liquid-fuel applications.<sup>[1-2]</sup> The produced bio-oil is also immiscible with conventional petroleum feedstocks and is unstable, polymerizing during storage.<sup>[3]</sup> Catalytic hydrodeoxygenation has been proposed as a technology to remove the oxygen content and increase the fuel value of bio-oil using traditional hydrotreating catalysts, NiMo and CoMo sulfides.<sup>[3-9]</sup> However, these catalysts often deactivate by several proposed mechanisms including coking, mineral deposition, phase change, and leaching.<sup>[10-12]</sup> In addition, fast pyrolysis of biomass creates hundreds of different compounds including organic acids, alcohols, furans, and large phenolic oligomers and hydrotreating of the resultant pyrolysis oil produces hundreds of different hydrocarbons alkanes from  $\text{C}_1$  to  $\text{C}_{24}$ .<sup>[3]</sup> The complex number of products makes understanding the basic chemistry that occurs during hydrodeoxygenation difficult.

Similar biomass conversion technologies, called Hydropyrolysis, have been proposed by Pindoria et al. and Marker et al.<sup>[13-14]</sup> They utilize sulfided NiMo and CoMo catalysts during the first pyrolysis step in the presence of hydrogen. Marker et al. reported that the Integrated Hydropyrolysis and Hydroconversion ( $\text{IH}^2$ ) was able to obtain yields up to 26 wt%  $\text{C}_4+$  on the 50 kg/day scale from maple wood biomass.<sup>[14-15]</sup> This technology is being commercialized by Shell and Criterion with a 5 ton/day demonstration facility in Bengaluru, India.<sup>[16]</sup> In this process, lignocellulosic biomass is pyrolyzed in a fluidized bed reactor in the presence of a sulfided, molybdenum based hydrotreatment catalyst followed by hydrotreatment in a secondary packed bed reactor. Figure 1 shows a simplified representation of the hydropyrolysis process. The hydropyrolysis in the first step allows for most of the oxygen to be removed before the reactive vapors can oligomerize, effectively stabilizing the pyrolysis intermediates. The light gases produced in this reaction are reformed to supply heat and generate the required hydrogen. Marker et al. has reported that the sulfided catalyst remained stable for 750 h time-on stream (TOS), with no information regarding a sulfur co-feed or any continuous regeneration.<sup>[14-15, 17]</sup>

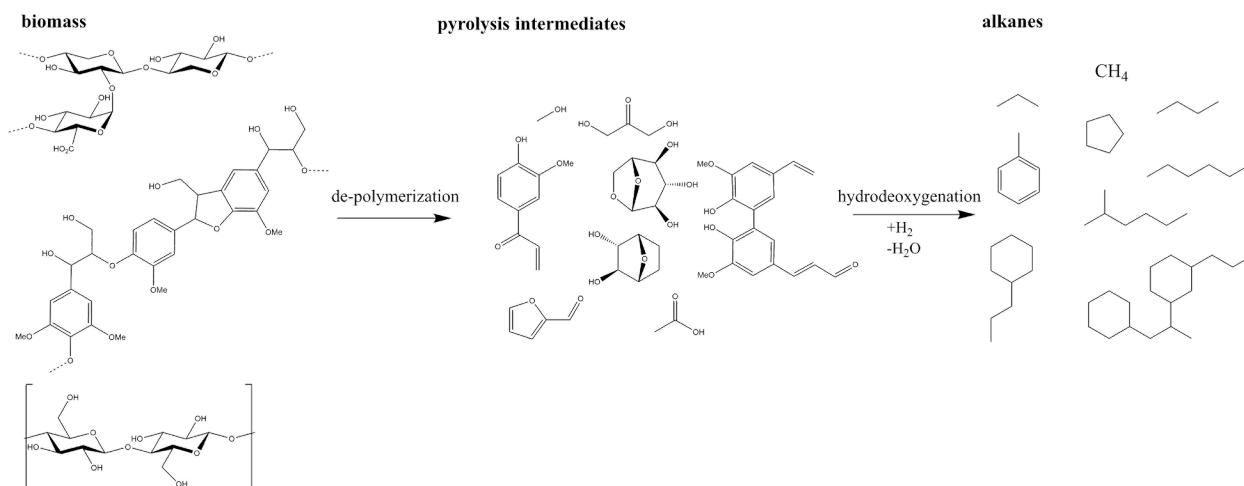


Figure 1: The overall process for the hydrodeoxygenation of lignocellulosic biomass, displaying the thermal depolymerization of biomass followed by the subsequent hydrodeoxygenation of resulting vapors.

Several other groups have published studies on the hydrodeoxygenation of lignocellulosic biomass in fluidized bed reactors using molybdenum based hydrotreatment catalysts.<sup>[18-21]</sup> Dayton et al. tested the hydrodeoxygenation of loblolly pine with a reduced NiMo/Al<sub>2</sub>O<sub>3</sub> catalyst showing non-aqueous C<sub>4</sub>+ yields as high as 24.1 wt% with an oxygen and moisture content of 2.4 and 2.5 wt% respectively. The catalyst stability was tested by 10 sequential 90 min experiments followed by oxidation and reduction, showing no major change in yield over these 10 experiments, yielding an average organic yield of 22.5 ± 1.35 wt% with an oxygen content of 2.8 ± 0.99 wt%.<sup>[18]</sup> Stummann et al. tested the hydrodeoxygenation of beech wood with sulfided NiMo/MgAl<sub>2</sub>O<sub>3</sub> and CoMo/MgAl<sub>2</sub>O<sub>3</sub> catalysts at 450°C and 26 bar, with C<sub>4</sub>+ organic yields varying between 24.3 and 26.4 wt% with an oxygen content of between 9.0 and 12 wt% on a dry basis. The stability of the catalysts were not explicitly tested, but the carbon content on the spent catalysts ranged from 0.9 and 3.3 wt% with 2.4 wt% potassium on the surface of the catalyst.<sup>[20]</sup> These empirical studies have shown the promise of sulfided Mo catalysts for conversion of biomass, yet few have reported fundamental studies on the hydrodeoxygenation of biomass with these catalysts.

Density functional theory (DFT) studies by Kasiraju et al. have shown hydrodeoxygenation (HDO) over a MoO<sub>3</sub> catalyst and hydrodesulphurization (HDS) over a MoS<sub>2</sub> catalyst follow similar mechanisms.<sup>[22]</sup> It has been proposed that the active site of a molybdenum based hydrotreatment catalyst is the vacancy of sulfur atoms on the surface, with nickel or cobalt atoms promoting the activity of these catalysts by forming bridge sites between the molybdenum and promoter atom at the edge.<sup>[23]</sup> A sulfur vacancy in the MoS<sub>2</sub> phase is active for heteroatom removal, but is stabilized and promoted by nickel or cobalt edge sites.<sup>[24-26]</sup> The main difference between the HDO and HDS mechanisms is the removal of the remaining oxygen or sulfur respectively by hydrogen.<sup>[22]</sup> Upon sulfiding, acid sites in the form of sulfhydryl groups can also form. Sulfur co-feeds

such as H<sub>2</sub>S, dimethyldisulfide (DMDS), dimethylsulfoxide (DMSO), or other liquid sulfiding agents are required during HDO to prevent removal of too much sulfur from the bulk.<sup>[24, 27]</sup>

HDO studies with model oxygenate studies show that the catalyst are stable when sulfur is co-fed, but these studies have typically been carried out at bio-oil hydrotreatment conditions (300°C and 200 bar) using oxygenate models with different effective carbon/hydrogen ratios than pyrolysis vapors.<sup>[28-32]</sup> The effective carbon/hydrogen ratio is used to describe the difficulty of upgrading a feedstock through hydrotreatment and takes into account the required hydrogen for hydrodeoxygenation.<sup>[32-33]</sup> Dabros et al. carried out HDO of ethylene glycol over NiMoS<sub>x</sub>, CoMoS<sub>x</sub>, and MoS<sub>x</sub> catalysts supported on MgAl<sub>2</sub>O<sub>3</sub> at 400°C and 27 bar H<sub>2</sub>, showing a reduction of over half of the conversion after 70 h TOS with a 550 ppm H<sub>2</sub>S co-feed. The stability of each catalyst was improved by increasing the H<sub>2</sub>S co-feed from 550 to 2200 ppm. The catalysts also showed high C-C bond cleavage with molar C<sub>2</sub>/C<sub>1</sub> ratios ranging from 1.5-4.8. Through XAS studies and model work, the improved stability was attributed to less exchange of the oxygen and sulfur on the surface with higher partial pressure of H<sub>2</sub>S and the use of Ni and Co promoters.<sup>[24]</sup> Limited work has been done on the activity and stability of sulfided hydrotreatment catalysts at hydrolysis conditions. Biomass hydrolysis consists of many sequential and parallel C-C cleavage, hydrogenation, deoxygenation, and C-C coupling steps. Saturated products are formed during this process by hydrotreatment, deoxygenation and hydrogenation with lighter products formed by C-C bond cleavage. Simple, but chemically similar model compounds must be used during model work to understand the reaction chemistry of hydrolysis. Due to several reaction types occurring during the HDO of polyoxygenates, more comprehensive metrics must be developed and utilized to explore the activity and stability of hydrotreatment catalysts for the hydrolysis of biomass.

The objective of this work was to measure the reaction rates of deoxygenation, C-C bond cleavage, and hydrogenation for HDO of glycerol over reduced and sulfided NiMo/Al<sub>2</sub>O<sub>3</sub> catalysts in a continuous flow reactor. During glycerol HDO, oxygen is removed, hydrogen is added, and C-C bonds are cleaved forming a variety of deoxygenated products as shown in Figure 2. These intermediates are similar to the products found during cellulose pyrolysis, making glycerol a good model for the cellulose and hemicellulose portion of biomass. Three conversions (all shown in Figure2) were developed to compare catalyst activity for glycerol HDO including the deoxygenation, hydrogenation and the C-C bond cleavage conversion. These metrics can be utilized in further biomass conversion studies to quantify various reaction types in a complicated reaction network. Glycerol has previously been used as a model to study the aqueous phase reforming of sugars and sugar alcohols<sup>[34]</sup> and was chosen as the feedstock for this study because it is thermally stable unlike pyrolysis oil or pyrolysis vapors. This work helps identify the role of sulfur on catalyst stability for hydrotreating catalysts and the mechanism of catalyst deactivation during HDO at hydrolysis conditions in a continuous flow reactor.

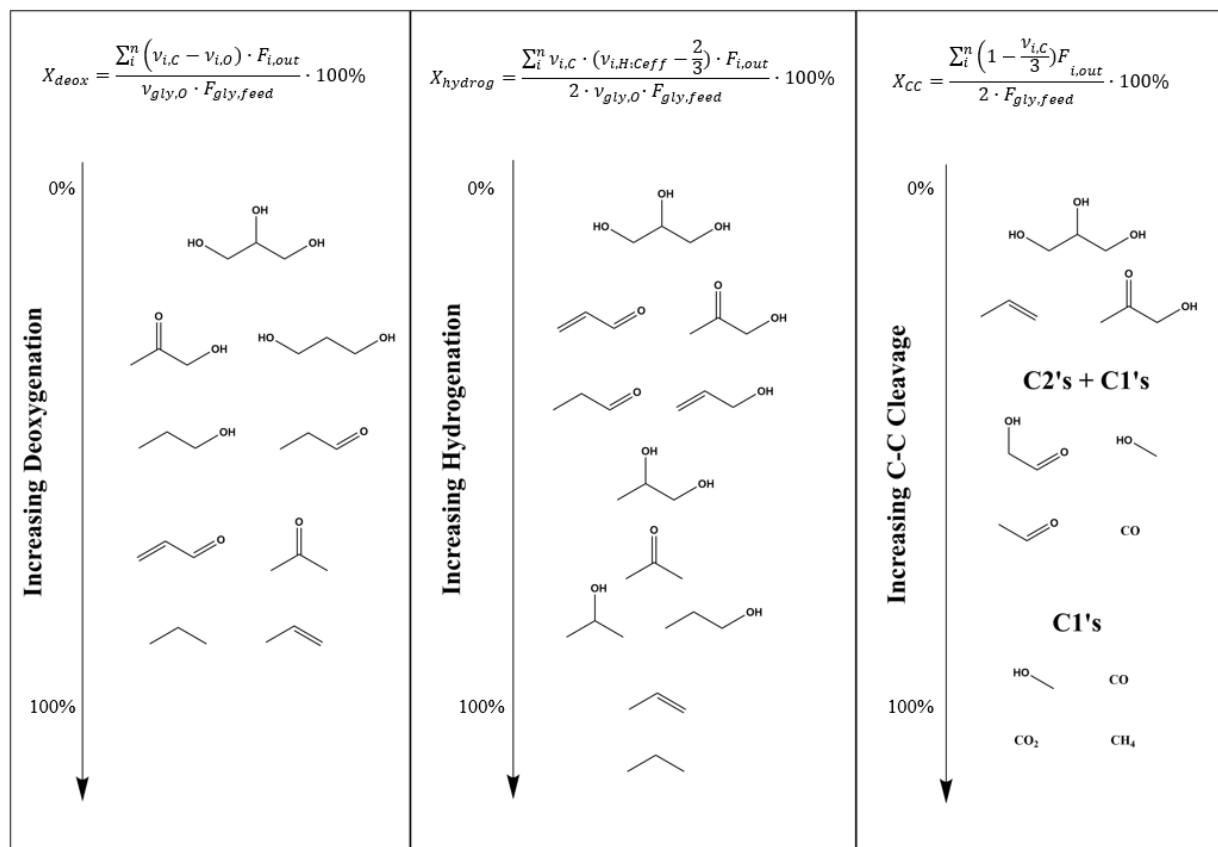


Figure 2: General scheme for glycerol HDO and the analysis used for measuring the relative activity of deoxygenation, hydrogenation, and C-C cleavage.

## 2. Results and Discussion

### 2.1. Glycerol HDO over NiMoS<sub>x</sub> and NiMoO<sub>x</sub> catalysts with varying H<sub>2</sub>S co-feeds

Figure 5 shows deoxygenation, hydrogenation, and C-C cleavage conversions along with the product yields as a function of TOS for glycerol HDO over NiMoO<sub>x</sub> with no H<sub>2</sub>S in the feed. The products are divided into three main categories: alkanes/alkenes, oxygenates, and CO<sub>x</sub>. The alkanes/alkenes consist of propane, propylene, ethane, ethylene, and methane. The oxygenates consist mainly of 1-propanol, allyl alcohol, propionaldehyde, acrolein, hydroxyacetone, acetaldehyde, ethanol, and methanol. The CO to CO<sub>2</sub> ratio is about 4:1. At 3.3 h TOS, the deoxygenation, hydrogenation, and C-C cleavage conversion are 82.5%, 62.9%, and 11.8% respectively. After 29.9 TOS these conversions all decrease to 43.1%, 18.7%, and 8.9% respectively. The products at 3.3 h TOS are highly deoxygenated and saturated compounds such as propane, propylene, and mono-alcohols demonstrating that NiMoO<sub>x</sub> is an active catalytic material for deoxygenation. As the catalyst deactivates, the extent of deoxygenation and hydrogenation is reduced and the major products are oxygenated compounds such as propionaldehyde, hydroxyacetone, and acrolein (Figure 5).

Figure 6 shows deoxygenation, hydrogenation, and C-C cleavage conversions along with the product yields with time on stream for glycerol HDO over NiMoS<sub>x</sub> with no H<sub>2</sub>S in the feed. At 3.3 h TOS, the deoxygenation and hydrogenation conversions are 70.2% and 42.3% respectively, lower than the values for HDO of glycerol over NiMoO<sub>x</sub> at the same conditions. The deoxygenation and hydrogenation conversions decrease to 39.3% and 12.3% respectively after 28.7 h TOS. The initial C-C cleavage conversion is higher for NiMoS<sub>x</sub> at 28.0% than NiMoO<sub>x</sub> at 11.8%. All products observed for glycerol HDO over NiMoS<sub>x</sub> are observed while using NiMoO<sub>x</sub>. The major difference between these two catalysts is the C-C cleavage activity, where NiMoO<sub>x</sub> produces 3.0% CO<sub>x</sub> initially while the NiMoS<sub>x</sub> produces 18.9% CO<sub>x</sub>. Regeneration of the NiMoS<sub>x</sub> catalyst was attempted by calcination up to 500°C and sulfiding following the procedure described in the experimental section. After deactivating to 62.2% of the initial deoxygenation activity, only 82.2% of the initial activity was returned after the first regeneration and the catalyst continued to deactivate quickly. A second regeneration resulted in only 63.1% of the initial deoxygenation activity.

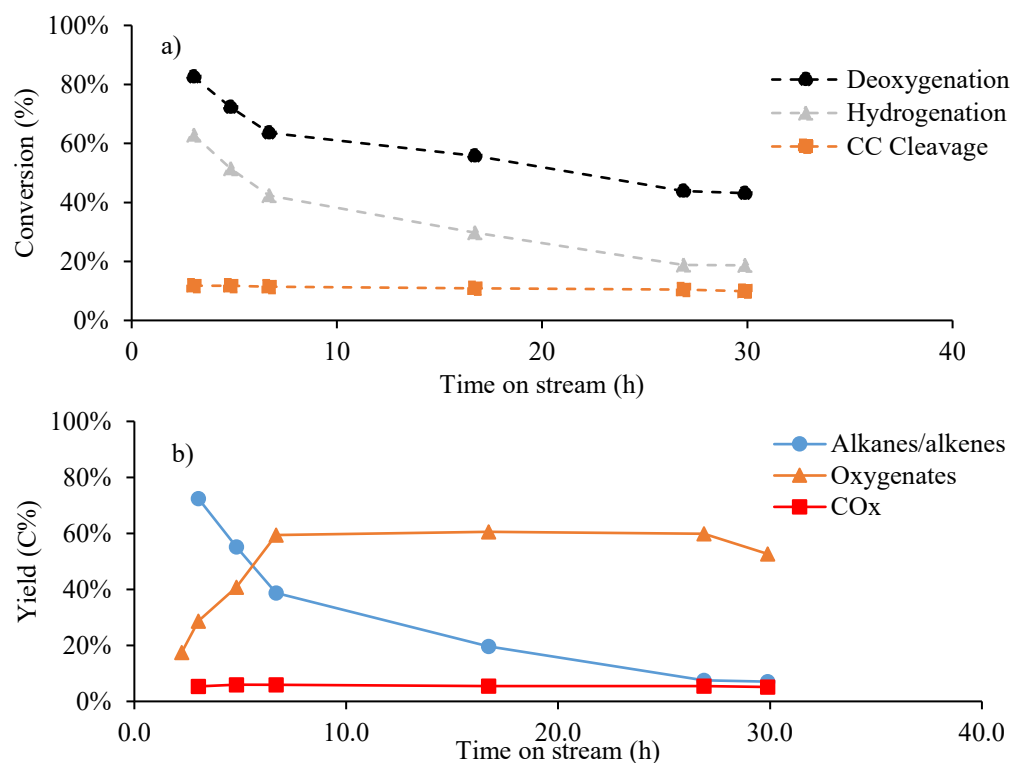


Figure 3: Glycerol HDO over NiMoO<sub>x</sub> catalyst with no sulfur co-feed. Reaction conditions: 400°C, 270 psig, contact time of 360 s.

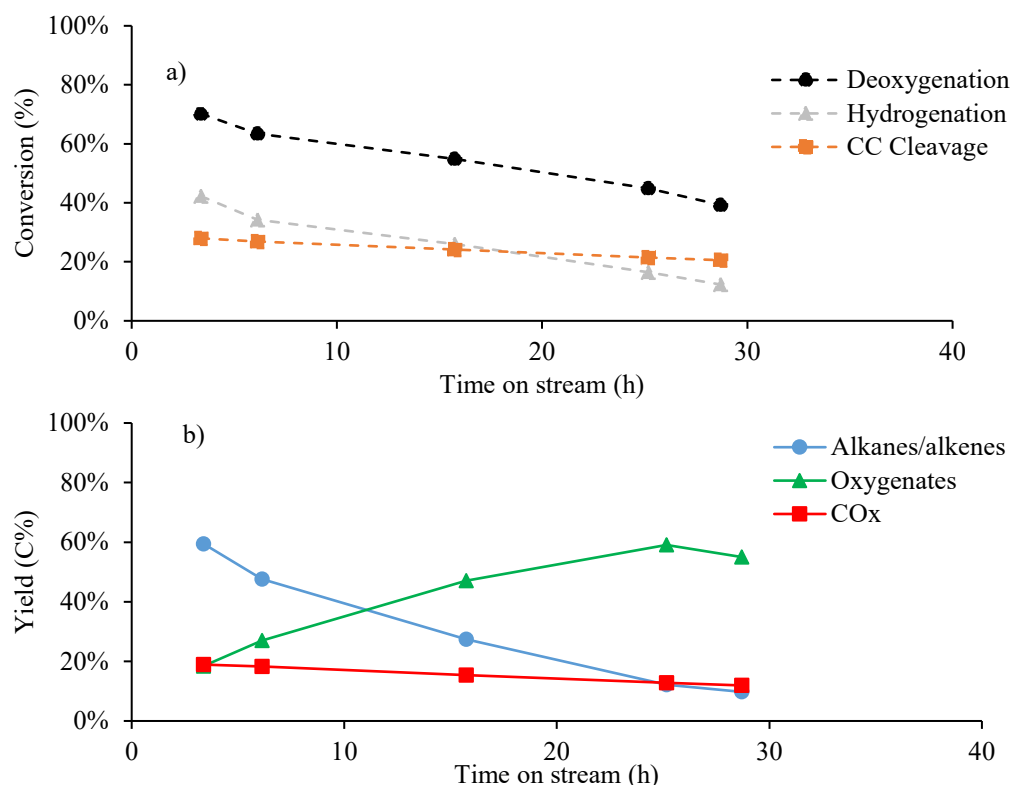


Figure 4: Glycerol HDO over NiMoS<sub>x</sub> catalyst with no sulfur co-feed. Reaction conditions: 400°C, 270 psig, contact time of 360 s.

Hydrogen sulfide gas was introduced in the reaction feed by co-feeding a gas stream of 2% H<sub>2</sub>S in H<sub>2</sub>. The first data points for these experiments were taken at about 3 h TOS as shown in Figure 7. The products when H<sub>2</sub>S was co-fed with the hydrogen were the same as the products without an H<sub>2</sub>S co-feed. At 3.0 h TOS, the deoxygenation and hydrogenation conversions are 82.7% and 72.5% respectively with a 2100 ppm H<sub>2</sub>S co-feed, showing higher hydrogenation activity than glycerol HDO with NiMoS<sub>x</sub> catalyst without an H<sub>2</sub>S co-feed. After 30.1 h TOS, the deoxygenation and hydrogenation decrease to 78.1% and 57.9%, respectively. The initial C-C cleavage conversion is 22.3%, lower than the 28.0% observed with no H<sub>2</sub>S co-feed. The C-C cleavage increases from 22.3% to 30.7% after 30.1 h TOS, in contrast to C-C cleavage decreasing over time without H<sub>2</sub>S co-feed.

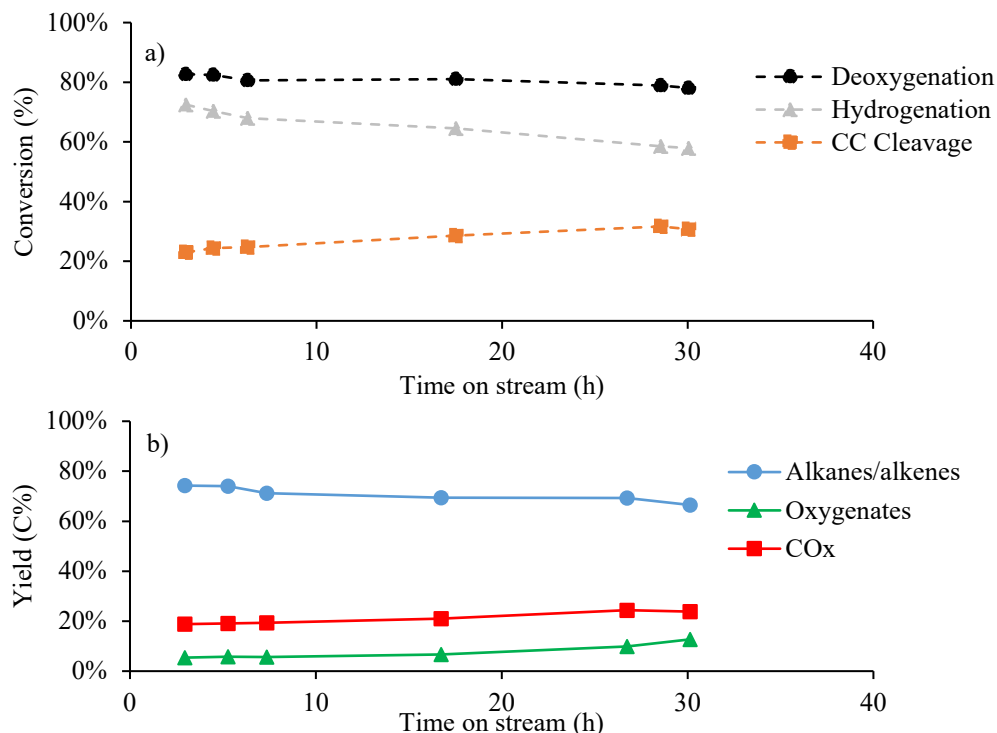


Figure 5: Glycerol HDO over NiMoS<sub>x</sub> catalyst with 2100 ppm H<sub>2</sub>S co-feed. Reaction conditions: 400°C, 270 psig, contact time of 360 s.

Table 2 shows the conversions, deactivation rate constants, and carbon yields for NiMoO<sub>x</sub> and NiMoS<sub>x</sub> with varying H<sub>2</sub>S co-feeds. The glycerol conversion is 100% for each experiment, but the deactivation rate constants were calculated from the deoxygenation, hydrogenation, and C-C cleavage conversions. Catalyst activities were not measured at low conversions, because at low glycerol conversion the unsaturated products condensed and low carbon balances were obtained. Without a sulfur co-feed, the deactivation rate constants for deoxygenation and hydrogenation for NiMoS<sub>x</sub> and NiMoO<sub>x</sub> are similar. However, NiMoS<sub>x</sub> has a higher deactivation rate constant for C-C cleavage than NiMoO<sub>x</sub>. When 700 and 2100 ppm H<sub>2</sub>S are added to the feed for NiMoS<sub>x</sub> catalyst the deoxygenation and hydrogenation deactivation rate constants reduce from 2.12E-2 and 4.50E-2 h<sup>-1</sup> (without H<sub>2</sub>S) to 1.3E-3 and 1.26E-2 h<sup>-1</sup> (with 700 ppm H<sub>2</sub>S) and 1.7E-3 and 7.6E-3 h<sup>-1</sup> (with 2100 ppm H<sub>2</sub>S), respectively. The deoxygenation and hydrogenation deactivation rate constants decreased by 10 and 5 times respectively when H<sub>2</sub>S was co-fed with glycerol. The added H<sub>2</sub>S increased the C-C cleavage activity with time giving negative C-C cleavage deactivation rate constants. This results in an increase in CO<sub>x</sub> and other C<sub>1</sub>/C<sub>2</sub> products with time on stream. The H<sub>2</sub>S thus plays three roles in the reaction: 1) increases the deoxygenation and hydrogenation activity, 2) reduces initial C-C cleavage and 3) increases the catalyst stability.

Table 1: Glycerol HDO over NiMoO<sub>x</sub> and NiMoS<sub>x</sub> catalyst with varying H<sub>2</sub>S co-feed, showing conversions and deactivation constants ( $\beta$ ). Reaction conditions: 400°C, 270 psig, 360 s contact time.

Catalyst	NiMoO <sub>x</sub>	NiMoS <sub>x</sub>	NiMoS <sub>x</sub>	NiMoS <sub>x</sub>
H <sub>2</sub> S (ppm)	0	0	700	2100
Conversion (%)	100	100	100	100
ToS (h)	3.0	3.3	2.9	3.0
Carbon Balance (%)	102.3	101.2	100.4	98.0
Deoxygenation (%)	82.5	70.2	77.4	82.7
$\beta_{1,deox}$ (h <sup>-1</sup> )*10 <sup>2</sup>	2.22	2.12	0.13	0.17
Hydrogenation (%)	62.9	42.3	58.8	72.5
$\beta_{1,hydrog}$ (h <sup>-1</sup> )*10 <sup>2</sup>	4.34	4.50	1.26	0.76
C-C Cleavage (%)	11.8	28.0	30.6	23.0
$\beta_{1,cc}$ (h <sup>-1</sup> )*10 <sup>2</sup>	0.59	1.21	-0.79	-1.07
C3:C2:C1	1:0.17:0.12	1:0.33:0.42	1:0.45:0.49	1:0.35:0.31
Carbon Yield (%)				
Alkanes/alkenes	72.4	59.5	74.3	80.2
Oxygenates	17.5	18.4	5.4	4.5
CO <sub>x</sub>	5.3	18.9	18.0	12.1
Unidentified	7.0	4.4	2.0	1.2

## 2.2. Glycerol HDO at varying contact times

Figure 8 shows the product yields for glycerol HDO without H<sub>2</sub>S co-feed over the NiMoS<sub>x</sub> catalyst with varying contact time. The deoxygenation and hydrogenation conversions increase with contact time, resulting in increasing alkane/alkene yields with contact time. Oxygenate yield appears to go through a maximum with contact time. C-C cleavage increases with contact time with a resulting increase in CO<sub>x</sub> yield. At a contact time of 360 s, the carbon balance was >98.0% with a fresh catalyst for all experiments. The products from glycerol HDO at contact times of 3 and 45 s were dark brown, indicating the formation of unidentifiable condensation products. At these same contact times the reactor plugged after 8 h TOS. Because of this, stability studies were not run at contact times of 3 and 45 s. A low carbon balance (80 % at 3 s) at lower contact time which may be due to the formation of oxygenates oligomers that are not detected using the analytical techniques in this study. These results highlight that the oxygenated intermediates produced from glycerol (a thermally stable molecule) are thermally unstable and can form oligomers during the reaction. This also complicates the identification of primary products.

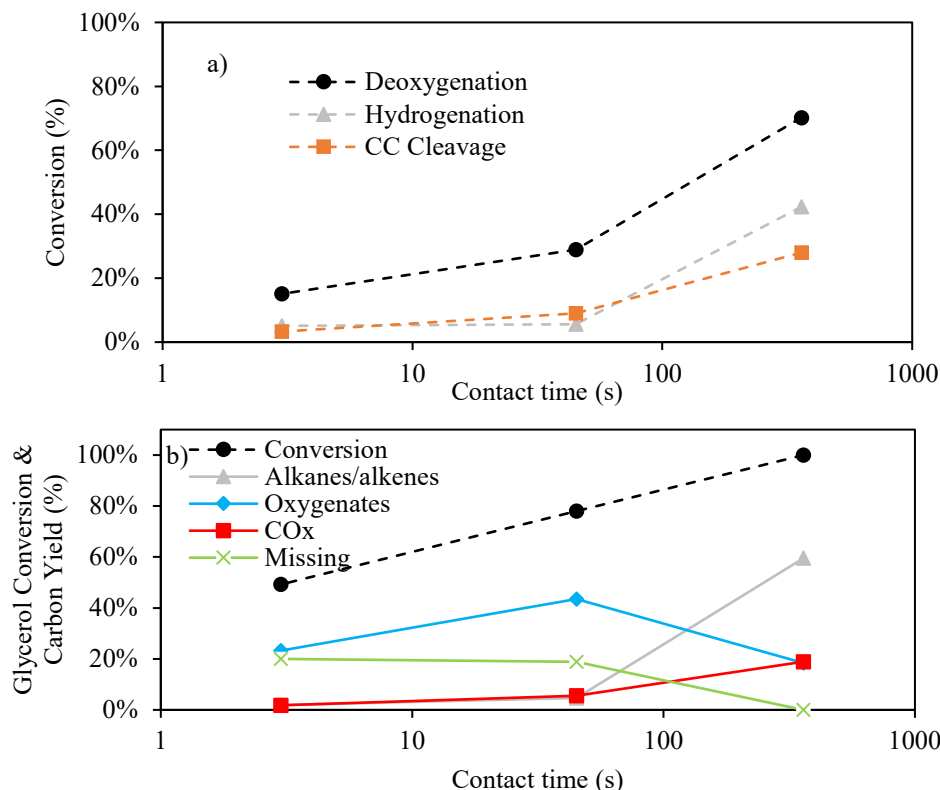


Figure 6: Glycerol HDO over NiMoS<sub>x</sub> catalyst with no H<sub>2</sub>S co-feed, showing conversions (a) and product yields (b) as a function of contact time. Reaction conditions: 400°C, 270 psig, contact times of 3-360 s, 3 h TOS.

Table 3 shows the product selectivities, normalized to 100%, for glycerol HDO over NiMoS<sub>x</sub> at contact times varying from 3 to 360 s with no sulfur co-feed and at a contact time of 3 s with a 2100 ppm H<sub>2</sub>S co-feed. The carbon balance for the 3 s contact time with the 2100 ppm H<sub>2</sub>S was higher than the carbon balance without the H<sub>2</sub>S co-feed. The selectivities at a contact time of 3 s without H<sub>2</sub>S are 24.6% allyl alcohol, 8.8% hydroxyacetone, 7.3% acrolein, and a missing carbon selectivity of 34.8%. At a contact time to 45 s the major product selectivities include 13.1% propionaldehyde, 11.9% hydroxyacetone, 11.1% acrolein, 8.9% allyl alcohol, 7.1% acetaldehyde, and a missing carbon selectivity of 17.4%. From 3 to 45 s, the hydrogenation conversion only slight increases. At a contact time of 360 s, the major products are mostly alkanes/alkenes, CO<sub>x</sub>, and saturated oxygenates with no missing carbon. The “others” group consists of condensation products such as ethers and acetals like 5-hydroxy-1,3-dioxane. At a contact time of 3 s with an H<sub>2</sub>S co-feed of 2100 ppm the selectivities were 41.4% allyl alcohol, 20.9% hydroxyacetone, 9.4% acrolein, 8.7% methanol, 7.7% propylene, 3.8% acetaldehyde, and no missing carbon. At a short contact time, adding H<sub>2</sub>S to the co-feed lowers the catalyst activity to deoxygenation, hydrogenation, and C-C cleavage while mitigating the loss of carbon through condensation reactions. This decrease in activity is likely due to inhibition by H<sub>2</sub>S.<sup>[25, 35]</sup> This result is in contrasts with the results at a contact time of 360 s (Table 2) where the run at 2100 ppm H<sub>2</sub>S shows higher activity than the run

at 0 ppm H<sub>2</sub>S. The higher activity with H<sub>2</sub>S at the longer contact time is likely due to the improved stability of the catalysts with H<sub>2</sub>S.

Table 2: Glycerol HDO over NiMoS<sub>x</sub> catalyst, showing conversions, product selectivity, and production rates with varying contact times. Reaction conditions: 400°C and 270 psig.

Contact time (s)	3	3	45	360	360
H <sub>2</sub> S (ppm)	2100	0	0	0	2100
Conversion (%)	5.5	49.2	76.0	100.0	100
Carbon Balance (%)	102.4	82.9	86.7	101.2	98.0
Deoxygenation (%)	4.2	15.6	31.4	70.2	82.7
Hydrogenation (%)	1.8	5.7	6.1	42.3	72.5
C-C Cleavage (%)	0.6	3.3	9.8	28.0	23.0
C3:C2:C1	1:0.06:0.08	1:0.06:0.09	1:0.15:0.17	1:0.33:0.42	1:0.35:0.31
Carbon Selectivity (%) [Production Rate (mmol Carbon h <sup>-1</sup> )]					
<b>Alkanes/alkenes</b>	<b>8.8[0.2]</b>	<b>3.9[0.7]</b>	<b>8.7[2.6]</b>	<b>58.9[22.8]</b>	<b>80.2[31.0]</b>
Propane	0.2[0.0]	0.0[0.0]	0.1[0.0]	16.5[6.4]	37.2[14.4]
Propylene	7.7[0.2]	3.5[0.7]	5.1[1.5]	26.0[10.1]	16.3[6.3]
Ethane	0.0[0.0]	0.1[0.0]	0.4[0.1]	11.0[4.3]	16.9[6.5]
Ethylene	0.2[0.0]	0.1[0.0]	0.8[0.2]	1.9[0.7]	0.2[0.1]
Methane	0.6[0.0]	0.2[0.0]	0.3[0.1]	3.5[1.4]	1.8[0.7]
<b>Oxygenates</b>	<b>91.1[1.9]</b>	<b>48.9[9.3]</b>	<b>57.6[17.0]</b>	<b>18.2[7.1]</b>	<b>4.5[1.7]</b>
1-Propanol	0.0[0.0]	0.0[0.0]	0.1[0.0]	4.4[1.7]	1.5[0.6]
Allyl alcohol	41.4[0.9]	24.6[4.7]	8.9[2.6]	2.8[1.1]	0.3[0.1]
Propionaldehyde	2.4[0.1]	1.5[0.3]	13.1[3.9]	1.6[0.6]	0.0[0.0]
Acrolein	9.4[0.2]	7.3[1.4]	11.1[3.3]	0.1[0.0]	0.0[0.0]
Acetone	2.7[0.1]	1.7[0.3]	2.5[0.7]	3.3[1.3]	0.2[0.1]
Hydroxyacetone	20.9[0.4]	8.8[1.7]	11.9[3.5]	0.0[0.0]	0.0[0.0]
Ethanol	1.9[0.0]	0.0[0.0]	0.4[0.1]	4.1[1.6]	1.1[0.4]
Acetaldehyde	3.8[0.1]	2.9[0.6]	7.1[2.1]	0.9[0.3]	0.0[0.0]
Methanol	8.7[0.2]	2.1[0.4]	2.5[0.7]	1.0[0.4]	1.39[0.5]
<b>CO<sub>x</sub></b>	<b>0.0[0.0]</b>	<b>3.7[0.7]</b>	<b>7.9[2.3]</b>	<b>18.7[7.2]</b>	<b>12.1[4.7]</b>
CO	0.0[0.0]	2.0[0.4]	6.8[2.0]	17.1[6.6]	11.1[4.3]
CO <sub>2</sub>	0.0[0.0]	1.7[0.3]	1.1[0.3]	1.6[0.6]	1.0[0.4]
<b>Others</b>	<b>0.2[0.0]</b>	<b>4.4[0.8]</b>	<b>5.7[1.7]</b>	<b>2.2[0.9]</b>	<b>1.2[0.5]</b>
<b>Missing</b>	<b>0.0[0.0]</b>	<b>34.8[6.6]</b>	<b>17.4[5.1]</b>	<b>0.0[0.0]</b>	<b>2.0[0.8]</b>

The proposed reaction pathway of glycerol HDO over a NiMoS<sub>x</sub> catalyst at hydrolysis conditions is shown in Figure 9. Glycerol first undergoes dehydration to produce either hydroxyacetone or 3-hydroxypropionaldehyde. Hydroxyacetone is observed as a major product at short contact times while 3-hydroxypropionaldehyde is observed below 0.1% carbon yields. These products can then be hydrogenated to produce 1,2 propanediol and 1,3 propanediol, respectively. 1,2 propanediol undergoes further dehydration forming acetone or allyl alcohol. Similarly 3-hydroxypropionaldehyde undergoes dehydration producing acrolein. Acrolein can then undergo hydrogenation to either propionaldehyde or allyl alcohol. Further hydrogenation and dehydration produces isopropanol, 1-propanol, propylene and propane. It is not clear when C-C cleavage occurs in this reaction pathway, however, acetaldehyde, ethanol, ethylene, ethane, CO, CO<sub>2</sub>, methanol, formaldehyde, and methane are all observed. C-C cleavage may occur through hydrogenolysis of glycerol to form ethylene glycol or 2-hydroxyacetaldehyde.<sup>[36-37]</sup> At short contact times, the major observed C<sub>2</sub> product was acetaldehyde with low yields of hydroxyacetaldehyde observed in some samples. Either acetaldehyde or hydroxyacetaldehyde could be formed through multiple C-C cleavage pathways. Since C<sub>2</sub> and C<sub>1</sub> are not observed in equimolar amounts, some C<sub>1</sub> products must be formed through C-C cleavage if C<sub>2</sub> products. At longer contact times, the C<sub>2</sub> products are mainly ethanol, ethylene, and ethane. The C<sub>3</sub> reaction pathway is less clear since the initial deoxygenation step occurs at either the primary or the secondary alcohol to form hydroxyacetone or 3-hydroxypropionaldehyde respectively. Hydroxyacetone is likely formed through direct dehydration or through the initial formation of glyceraldehyde, dehydration, and hydrogenation.<sup>[36, 38]</sup> Hydroxyacetone was observed as a major product at short contact times while 3-hydroxypropionaldehyde was only observed in small (<0.1% yield) quantities. 3-hydroxypropionaldehyde likely rapidly deoxygenates to form acrolein. Allyl alcohol was found to form selectively at a contact time of 3 s with and without a sulfur co-feed. Allyl alcohol could be formed through the hydrodeoxygenation of hydroxyacetone, the hydrodeoxygenation of hydroxypropionaldehyde, or the hydrogenation of acrolein. Some studies have shown selective production of allyl alcohol from glycerol claiming a hydrogen transfer mechanism where glycerol transfers hydrogen to acrolein to form allyl alcohol selectively.<sup>[39-41]</sup> Future research is needed to measure the rates of these individual pathways but Figure 9 provides the general products and suggested pathway from glycerol hydrodeoxygenation.

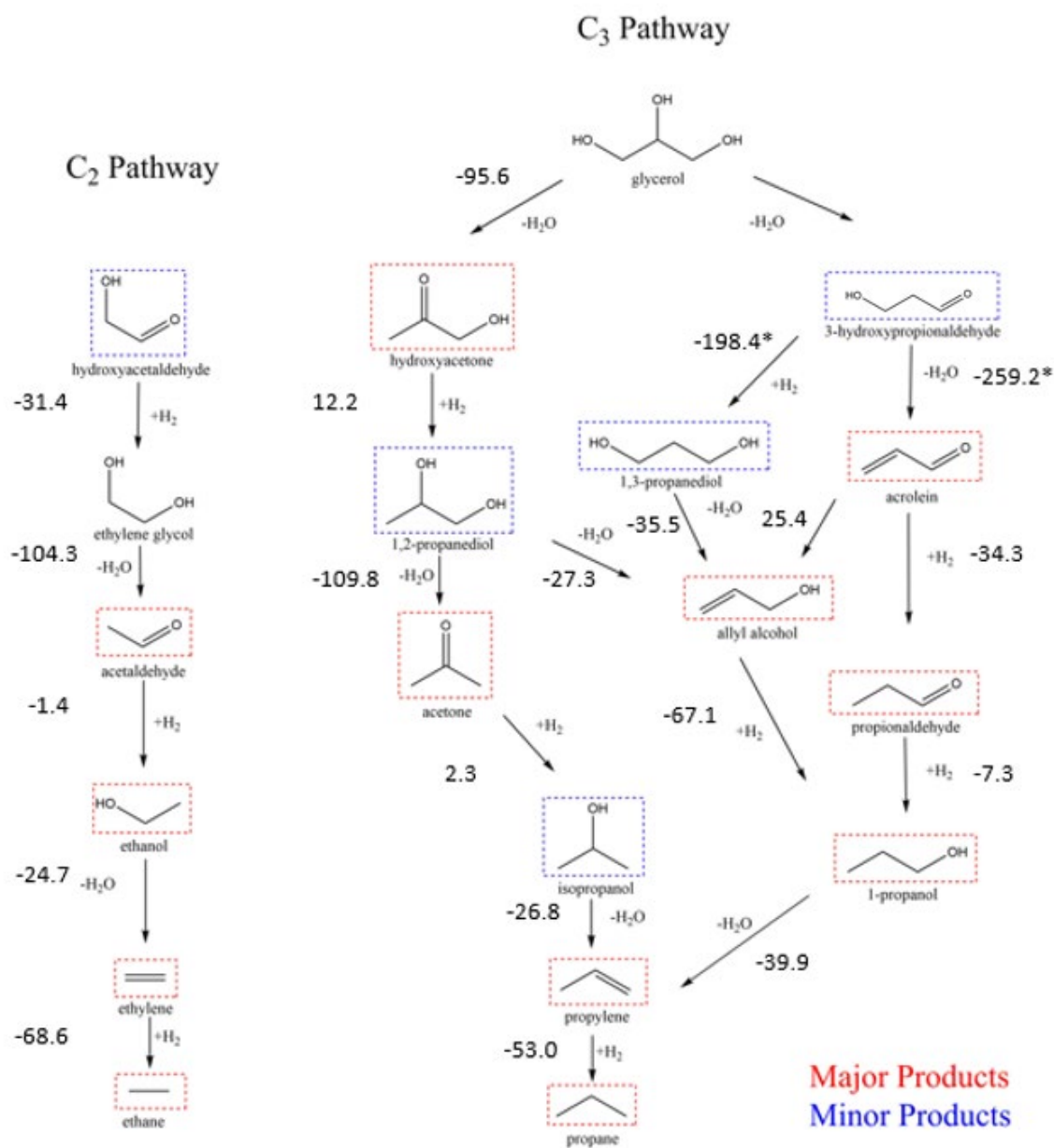


Figure 7: Proposed reaction network of glycerol HDO at hydropyrolysis conditions over a NiMoS<sub>x</sub> catalyst with the Gibbs free energies in kJ/mol calculated at 400°C. \*Values are calculated based on the formation from glycerol.

DMSO can also be used as a sulfiding agent for laboratory studies for hydrotreating catalysts.<sup>[27]</sup> Table 4 shows the product comparison at 3 and 360 s contact times for glycerol HDO with a DMSO co-feed, an H<sub>2</sub>S co-feed, and no H<sub>2</sub>S co-feed. DMSO is used as a non-toxic sulfiding agent in hydrotreating reactions as it is converted to H<sub>2</sub>S, water, and methane over a catalyst in a H<sub>2</sub> atmosphere.<sup>[27, 42]</sup> The DMSO experiments contained enough DMSO to produce 2100 ppm H<sub>2</sub>S if all DMSO was converted into methane, water, and H<sub>2</sub>S. At 360 s the carbon balances of no co-feed, H<sub>2</sub>S co-feed, and DMSO co-feed all show high carbon balances. Co-feeding DMSO as a sulfiding agent resulted in a 4 times higher deoxygenation deactivation constant and a 2 times higher hydrogenation deactivation constant compared with co-feeding H<sub>2</sub>S gas at 2100 ppm. At a short contact time, DMSO as a co-feed resulted in a carbon balance of 59.2%. The major product was acrolein, with only a small amount of allyl alcohol compared to the other experiments at 3 s. This low carbon balance was due to DMSO thermally decomposing into methylmercaptan and formaldehyde and homogeneously reacting with glycerol and other intermediates. This hypothesis was confirmed through an experiment with no catalyst at the same conditions where the glycerol conversion was 52.3% with a carbon balance of 64.5%. These experiments show that H<sub>2</sub>S is required to study NiMoS<sub>x</sub> catalysts at low conversion with oxygenated feeds.

Table 3: Glycerol HDO over NiMoS<sub>x</sub> catalyst with and without sulfur co-feeds (2100 ppm H<sub>2</sub>S equivalent), showing conversion and product yields with varying contact times. Reaction conditions: 400°C, 270 psig, 72.5-80 wt% glycerol and 0-7.5% DMSO in water

Co-feed	DMSO	H <sub>2</sub> S gas	None	DMSO	H <sub>2</sub> S gas	None
Contact time (s)	3	3	3	360	360	360
Conversion (%)	57.5	5.5	49.2	100.0	100.0	100.0
Carbon Balance (%)	59.2	102.4	82.9	106.2	98.0	101.2
Deoxygenation (%)	5.3	4.2	15.6	88.2	82.7	70.2
Hydrogenation (%)	2.9	1.8	5.7	73.6	72.5	42.3
C-C Cleavage (%)	0.8	0.6	3.3	25.4	23.0	28.0
$\beta_{1,deox}$ (h <sup>-1</sup> )*10 <sup>2</sup>	-	-	-	0.57	0.17	2.12
$\beta_{1,hydrog}$ (h <sup>-1</sup> )*10 <sup>2</sup>	-	-	-	1.28	0.76	4.50
$\beta_{1,cc}$ (h <sup>-1</sup> )*10 <sup>2</sup>	-	-	-	-0.36	-1.07	1.21
C3:C2:C1	1:0.11:0.09	1:0.06:0.08	1:0.06:0.09	1:0.37:0.32	1:0.35:0.29	1:0.33:0.42
Carbon Yield (%)						
<b>Alkanes/alkenes</b>	<b>0.6</b>	<b>0.5</b>	<b>1.9</b>	<b>84.5</b>	<b>80.2</b>	<b>59.5</b>
Propane	0.0	0.0	0.0	38.4	51.0	16.7
Propylene	0.1	0.4	1.7	20.0	5.4	26.3
Ethane	0.1	0.0	0.0	19.1	18.2	11.1
Ethylene	0.1	0.0	0.1	0.5	0.1	1.9
Methane	0.4	0.0	0.1	6.5	5.5	3.5
<b>Oxygenates</b>	<b>7.8</b>	<b>6.8</b>	<b>23.2</b>	<b>6.4</b>	<b>4.5</b>	<b>18.4</b>
1-Propanol	0.4	0.0	0.0	2.6	1.3	4.4
Allyl alcohol	0.3	2.3	12.1	0.0	0.1	2.9
Propionaldehyde	0.2	0.1	0.0	0.1	0.0	1.6
Acrolein	5.1	1.7	3.6	0.0	0.0	0.1
Acetone	0.2	0.7	0.8	0.3	0.6	3.3
Hydroxyacetone	0.8	1.4	4.3	0.0	0.0	0.0
Ethanol	0.0	0.1	0.0	3.4	2.0	4.2
Acetaldehyde	0.7	0.3	1.4	0.0	0.2	0.8
Methanol	0.1	0.5	1.0	0.0	0.3	1.0
<b>CO<sub>x</sub></b>	<b>0.1</b>	<b>0.0</b>	<b>1.8</b>	<b>13.1</b>	<b>12.1</b>	<b>18.9</b>
CO	0.1	0.0	0.9	12.2	11.5	17.3
CO <sub>2</sub>	0.0	0.0	0.8	0.9	0.6	1.6
<b>Unidentified</b>	<b>8.2</b>	<b>0.6</b>	<b>2.2</b>	<b>2.2</b>	<b>1.2</b>	<b>2.2</b>
<b>Missing</b>	<b>40.8</b>	<b>0.0</b>	<b>19.9</b>	<b>0.0</b>	<b>2.0</b>	<b>0.0</b>

### 2.3 Catalyst characterization

The BET surface areas and carbon content of fresh and spent catalysts after 30 h of glycerol HDO are shown in Table 5. The carbon content was calculated based on temperature programmed oxidation (TPO) and quantification of the resulting CO<sub>2</sub> and CO over time. The BET surface area of the fresh NiMoS<sub>x</sub> after sulfiding and passivation was 143.7 m<sup>2</sup>/g. The spent catalyst after glycerol HDO with no H<sub>2</sub>S co-feed had a BET surface area of 60.4 m<sup>2</sup>/g with a carbon content of 23.45% while the spent catalyst from the glycerol HDO experiment with 2100 ppm had a BET surface area of 81.2 m<sup>2</sup>/g with a carbon content of 1.93%. The carbon content difference indicates the deactivation could be largely caused by coking since the deactivation of NiMoS<sub>x</sub> was much higher with no H<sub>2</sub>S co-feed than with 2100 ppm H<sub>2</sub>S. The coking could be occurring due to a phase change on the catalyst surface caused by removal of sulfur from the MoS<sub>x</sub> basal plane.<sup>[22, 24]</sup> No bulk phase change was observed by XRD of the fresh and spent NiMoS<sub>x</sub>.

Figure 10 shows the results from TPO of the spent catalyst after 30 h TOS of glycerol HDO with 0 ppm H<sub>2</sub>S co-fed. The sulfur was removed by 350°C while the carbon was not removed until 500°C. The spent catalyst after 30 h TOS of glycerol HDO with 2100 ppm H<sub>2</sub>S co-feed showed 11% more SO<sub>2</sub> per gram catalyst during TPO than the catalyst from the 0 ppm H<sub>2</sub>S run at the same reaction and TPO conditions. During cooling of the spent catalyst after reaction, argon was flowed to remove any physisorbed H<sub>2</sub>S from the catalyst surface. This may indicate that one deactivation mechanism of the catalyst is loss of sulfur. Minor loss of sulfur and a large decrease in activity is consistent with loss of sulfur from just the Ni-Mo-S edge sites.<sup>[43]</sup> After multiple glycerol HDO reactions followed by three total regenerations through calcination and sulfiding, the surface area of the NiMoS<sub>x</sub>/Al<sub>2</sub>O<sub>3</sub> was 128.1 m<sup>2</sup>/g. This loss of surface area could be due to sintering of the active NiMoS<sub>x</sub> planar structure manifested in a loss of surface area and active Ni-Mo-S edge sites.<sup>[24, 44-45]</sup> High temperature calcination may also cause a change in the NiMoO<sub>x</sub> structure resulting in a less active NiMoS<sub>x</sub> catalyst upon sulfiding.<sup>[46]</sup>

Table 4: Characterization of NiMoS<sub>x</sub> catalyst before and after Glycerol HDO run for 30 h at a contact time of 360 s.

Catalyst	BET Surface Area (m <sup>2</sup> /g)	Carbon (wt%)
Fresh NiMoS <sub>x</sub>	143.7	-
Spent NiMoS <sub>x</sub> (2100 ppm H <sub>2</sub> S)	81.2	1.93%
Spent NiMoS <sub>x</sub> (0 ppm H <sub>2</sub> S)	60.4	23.45%
Regenerated NiMoS <sub>x</sub>	128.1	-

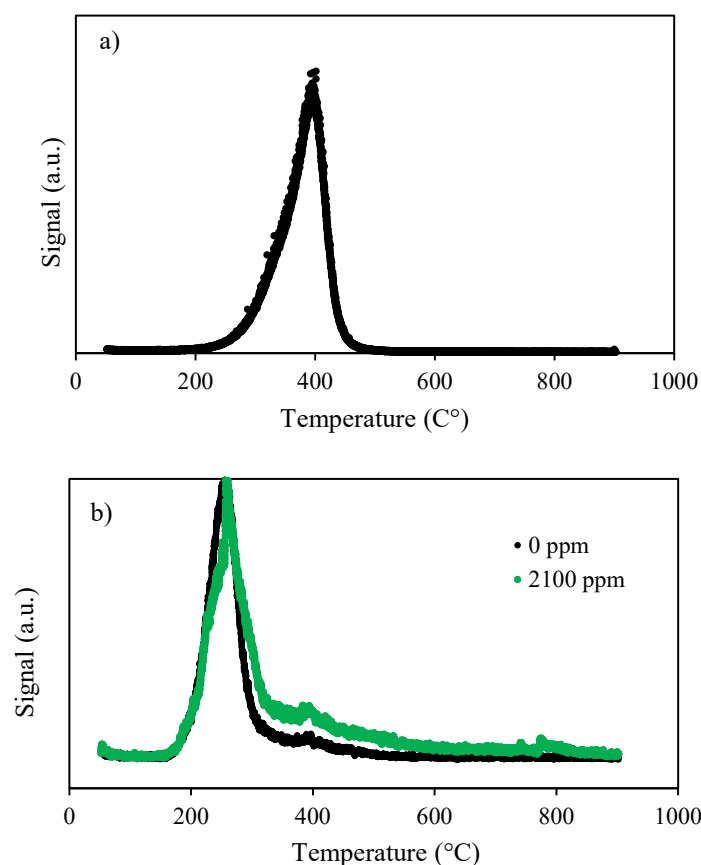


Figure 8: MS signal for a) 44 m/z (CO<sub>2</sub>) and b) 64 m/z (SO<sub>2</sub>) during the temperature programmed oxidation (TPO) of spent NiMoS<sub>x</sub> catalysts after 30 h of glycerol HDO with a 0 and 2100 ppm co-feed at a contact time of 360 s. Conditions: 50 mL/min of 10% O<sub>2</sub> in He at 1°C/min.

### 3. Conclusions

Standard NiMo hydrotreating catalysts can catalyze several classes of reactions for conversion of oxygenated biomass feedstocks including dehydration, C-C cleavage, deoxygenation, and hydrogenation. The major products of glycerol hydrodeoxygenation at short contact times were found to be unsaturated oxygenates including allyl alcohol, acrolein, hydroxyacetone, and acetaldehyde. The major products at longer contact times were alkanes/alkenes, CO<sub>x</sub>, and saturated alcohols such as propylene, propane, ethylene, methane, CO, methanol, ethanol, and 1-propanol. The initial rates of deoxygenation and hydrogenation for glycerol were found to be lower for a NiMoS<sub>x</sub> catalyst compared to the NiMoO<sub>x</sub> catalyst. The initial rate of C-C cleavage was higher for the NiMoS<sub>x</sub> catalyst compared to the NiMoO<sub>x</sub> catalyst. The NiMoS<sub>x</sub> and NiMoO<sub>x</sub> catalyst both deactivate at similar rates when no sulfur is added in the feed. The deactivation rate constants decreases according to the following order: hydrogenation > deoxygenation > C-C cleavage. The catalyst stability improves when sulfur is added to the feed as either H<sub>2</sub>S or DMSO. DMSO decomposes and reacts homogeneously with glycerol to form condensation products at short contact times resulting in a low carbon balance. Co-feeding H<sub>2</sub>S during hydrodeoxygenation improved the stability of the deoxygenation and hydrogenation activities up 12 and 6 times respectively, while the C-C cleavage deactivation rate constant becomes negative, resulting in an increase in C-C cleavage activity over time with an H<sub>2</sub>S co-feed. A major cause of deactivation is carbon deposition. The carbon content of spent NiMoS<sub>x</sub> catalysts after 30 h of glycerol HDO with 0 and 2100 ppm H<sub>2</sub>S in the feed were 23.45 and 1.93 wt% respectively, resulting in BET surface area reductions of 43.5% and 58.4% of the fresh NiMoS<sub>x</sub> catalyst surface. At a shorter contact time, the activity of the NiMoS<sub>x</sub> catalyst was lower when 2100 ppm H<sub>2</sub>S was co-fed compared to no sulfur co-feed, but resulted in a significantly improved carbon balance.

## 4. Experimental Section:

### Catalyst preparation:

A low NiMo catalyst supported on  $\gamma$ -alumina from Albemarle Catalyst Company was received in the oxide state and was used in either a reduced or sulfided state. The NiMoO<sub>x</sub> catalyst was reduced under H<sub>2</sub> flow at 270 psi and ramped at 1°C min<sup>-1</sup> to the 400°C reaction temperature prior to reaction. The NiMoS<sub>x</sub> catalyst was sulfided as instructed by the catalyst vendor. The catalyst was pretreated in batches in a H<sub>2</sub>S/H<sub>2</sub> atmosphere by flowing 4 wt% dimethyl disulfide (DMDS) in heptane with an Eldex Optos Model 1 piston pump at a WHSV of 2 h<sup>-1</sup> and H<sub>2</sub> gas at a GHSV of 600 h<sup>-1</sup> while carefully ramping the temperature as follows: hold for 3 h at 25°C, ramp to 250°C over 7.5 h, hold for 8 h, ramp to 320°C over 3.5 h, and hold for 6 h. Afterwards, the catalyst was cooled under argon flow to room temperature where the sulfided catalyst was passivated with air before removing from the reactor. Prior to every experiment with NiMoS<sub>x</sub>, the passivated catalyst was heated at 1°C min<sup>-1</sup> and held at 400°C for 1 h with 4 wt% DMDS in heptane pumped at a WHSV of >2 h<sup>-1</sup> and H<sub>2</sub> gas at a GHSV of at least 600 h<sup>-1</sup>.

### Catalyst characterization:

The spent catalysts were characterized via temperature-programmed oxidation (TPO) using a Micrometrics AutoChem II 2920 instrument equipped with a Cirrus 2 Quadrupole Mass Spectrometer. During TPO, 50 mg of catalyst was loaded into a quartz u-tube and dried for 2 h at 150°C with 50 mL min<sup>-1</sup> He flow. After cooling to room temperature, the sample was heated at a rate of 10°C min<sup>-1</sup> to 700°C with 50 mL min<sup>-1</sup> of 10% O<sub>2</sub> in He. The CO<sub>2</sub>, CO, and SO<sub>2</sub> were detected using mass spectrometry. The CO<sub>2</sub> and CO were calibrated to quantify the carbon from oxidation through integration. The surface area before and after reaction was determined by the Brunauer-Emmett-Teller (BET) method using a Micrometrics ASAP 2020 Plus instrument.

### Experimental setup:

A fixed bed reactor was used to carry out gas phase glycerol hydrodeoxygenation (HDO) as shown in Figure 9. Reactors were made with ¼" in diameter and 0.014" wall thickness 316L stainless steel tubing. For a typical reaction, 130 mg of catalyst was placed in the middle of a 10" long reactor between quartz wool and silica chips. The contact time (reported in seconds) of the glycerol reactant flowrate ( $g_{\text{feed}} \text{ s}^{-1}$ ) over the NiMo catalyst ( $g_{\text{cat}}$ ) was varied by changing the catalyst amount. For experiments at a contact time of 3 s, the catalyst was diluted 50 times with 40-60 mesh crushed silica. Experiments with < 100 mg of catalyst used catalyst diluted with silica chips ground and sieved to the same particle size as the NiMoS<sub>x</sub>/Al<sub>2</sub>O<sub>3</sub>. A glycerol HDO experiment with only silica chips was run and showed a carbon balance of 98.6% with no observed products. The catalyst was pretreated prior to the run according to the conditions in the catalyst preparation section. Once reaction conditions were met, the reaction was started by pumping 80% glycerol in water via an Eldex Optos Model 1 piston pump and flowing a mixture of ultrahigh purity (UHP) grade H<sub>2</sub> (Airgas) and 2% H<sub>2</sub>S in H<sub>2</sub> (Airgas) using two mass flow controllers

(Brooks). Liquid samples were collected from a pressurized collection vessel cooled to 0°C about every 2 h after the start of a reaction. The first liquid sample is transient and is not analyzed. The gas stream was sampled every 2 h, before every liquid sample. The spent catalyst was cooled to ambient temperature, purged with ultrahigh purity (UHP) grade Argon (Airgas) and passivated with air by flowing ultrahigh purity (UHP) grade air (Airgas) at 50 mL min<sup>-1</sup> for 30 min prior to removal from the reactor. The partial pressures, temperature and contact times used in this study are shown in Table 1 and are similar to those used in the IH<sub>2</sub> process.<sup>[14-15, 47]</sup> The total pressure was constant across all experiments, while the ranges of partial pressures shown vary due to differences in the conversion of glycerol, formation of water, H<sub>2</sub> consumption, and the amount of H<sub>2</sub>S fed.

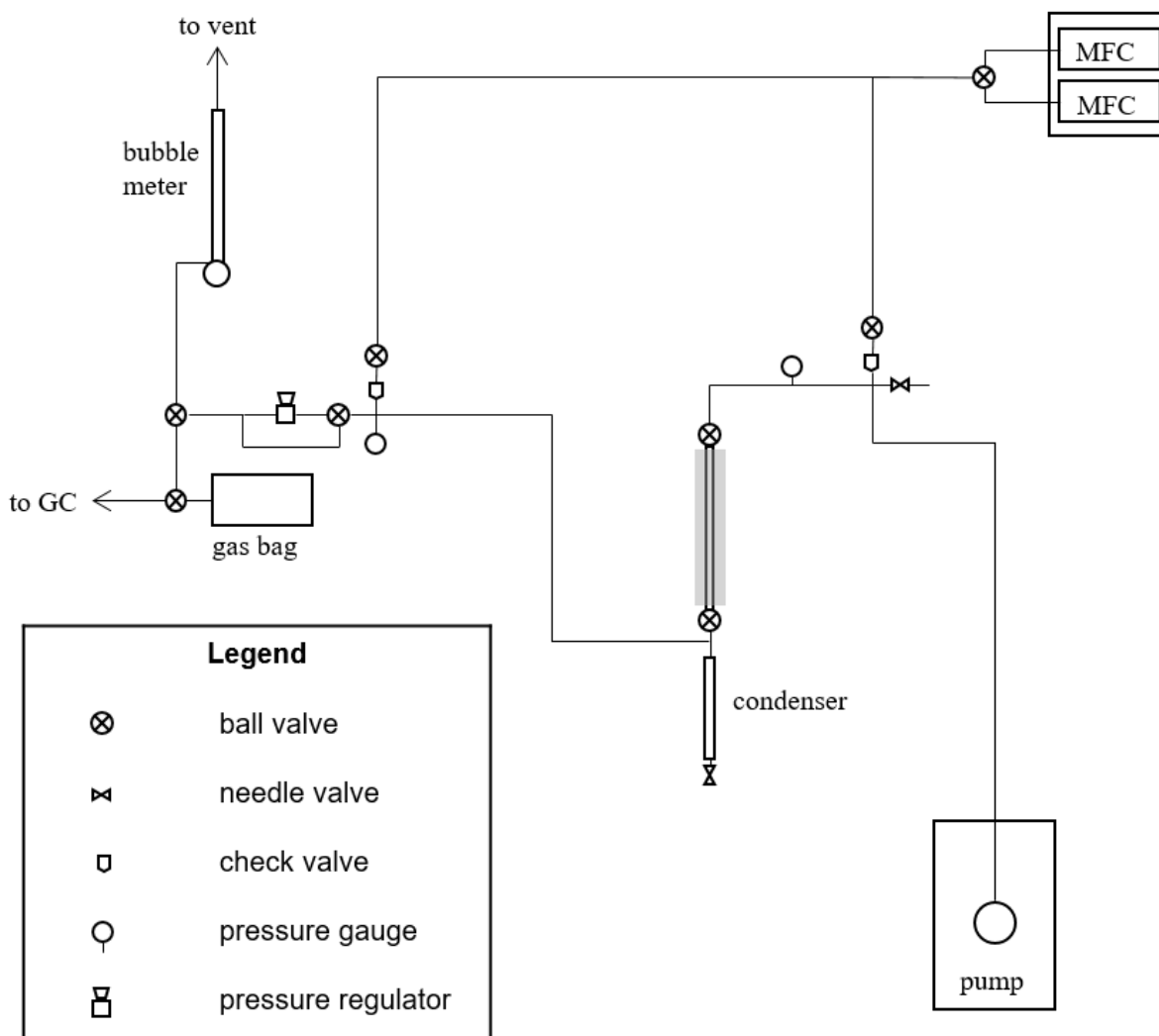


Figure 9: A simplified schematic of the packed bed flow reactor used for the continuously fed hydrodeoxygenation of glycerol at hydrolysis conditions.

Table 5: The process conditions for the hydrodeoxygenation (HDO) of glycerol at hydrolysis conditions.

<b>Process Condition</b>	
Temperature (°C)	400
Pressure (psig)	270
Hydrogen pressure (psi)	263-278
Water pressure (psi)	3-14
H <sub>2</sub> S pressure (psi)	0.0-0.6
Glycerol pressure (psi)	0-3
Gas residence time (s)	1

### Product analysis:

Gas samples were analyzed by an online Shimadzu GC-2014 instrument equipped with a sample loop and both a thermal conductivity detector (TCD) and flame ionization detector (FID). The TCD detector was used to quantify CO and CO<sub>2</sub> while the FID detector was used to quantify C1-C3 hydrocarbons and oxygenates. Permanent gases were identified and calibrated with triplicate single point calibration using SCOTTY specialty gas mixtures. Volatile oxygenates were identified by gas bag injection and quantified using the effective carbon number (ECN) and their respective carbon number alkane. samples were diluted by 8 times in water and by 5 times in tetrahydrofuran (THF) before analysis.<sup>[48]</sup> Liquid samples were identified using a Shimadzu GC-2010 instrument with a RTX-VMS column equipped with a Shimadzu GCMS-QP2010 mass spectrometer and quantified using a Shimadzu GC-2010 instrument equipped with a FID and RTX-VMS column.

The conversion of glycerol,  $X_{gly}$ , was calculated according to Equation 1 where  $F_{gly,feed}$  is the molar flow rate of glycerol into the reactor and  $F_{gly,prod}$  is the molar flow rate of glycerol out of the reactor. The carbon yield of any product  $i$ ,  $Y_i$ , is described in Equation 2 where  $\nu_{i,C}$  is the number of carbon atoms in product  $i$  and  $F_{i,out}$  is the molar flow rate of product  $i$ . The carbon balance,  $Y_{CBal}$  is described in Equation 3 which is calculated based on the total carbon fed into the system as glycerol and the gas and liquid products measured by GC-FID, where  $n$ , is the total number of products. Due to experimental error, a carbon balance slightly above 100% is not uncommon. We have introduced a variety of other conversions to analyze the complex products that are occurring in this reaction. The deoxygenation conversion,  $X_{deox}$ , is described in Equation 4 and is a molar conversion of C-O bonds cleaved in glycerol based on the observed gas and liquid products where  $\nu_{i,O}$  is the number of oxygen atoms in the product. The deoxygenation metric ranges from

0 to 100%, where 100% deoxygenation would indicate that 100% of the C-O bonds in glycerol were cleaved, resulting in a carbon yield of 100% alkane/alkene products. The hydrogenation conversion,  $X_{hydrog}$ , is described in Equation 5 and is a molar conversion of hydrogenations based on the amount of hydrogen in the observed gas and liquid products and the number hydrogenation events required to convert glycerol to propane.  $\nu_{i,H}$  is the number hydrogen atoms in product  $i$  and  $\nu_{gly,H}$  is the number of hydrogen atoms in glycerol. This metric ranges from 0 to 166.6 %, where 100% hydrogenation conversion indicates glycerol being converted to water and propane, and 166.6% hydrogenation indicates glycerol being converted to water and methane. The C-C cleavage conversion,  $X_{CC}$ , is described in Equation 6 which is a molar conversion of C-C bonds in glycerol based on the observed gas and liquid products. This metric ranged from 0 to 100%, where 100% C-C cleavage conversion indicates 100% of the C-C bonds in glycerol were cleaved to form all C1 products.

$$X_{gly} = \frac{F_{gly,feed} - F_{gly,prod}}{F_{gly,feed}} \cdot 100\% \quad (1)$$

$$Y_i = \frac{\nu_{i,C} \cdot F_{i,out}}{3 \cdot F_{gly,feed}} \cdot 100\% \quad (2)$$

$$Y_{CBal} = \frac{\sum_i^n \nu_{i,C} \cdot F_{i,out}}{3 \cdot F_{gly,feed}} \cdot 100\% \quad (3)$$

$$X_{deox} = \frac{\sum_i^n (\nu_{i,C} - \nu_{i,O}) \cdot F_{i,out}}{3 \cdot F_{gly,feed}} \cdot 100\% \quad (4)$$

$$X_{hydrog} = \frac{\sum_i^n 0.5 \cdot \nu_{i,C} \cdot (\nu_{i,H} \cdot C_{eff} - \frac{2}{3}) \cdot F_{i,out}}{3 \cdot F_{gly,feed}} \cdot 100\% \quad (5)$$

$$X_{CC} = \frac{\sum_i^n (1 - \frac{\nu_{i,C}}{3}) \cdot F_{i,out}}{2 \cdot F_{gly,feed}} \cdot 100\% \quad (6)$$

The rate of deactivation was approximated with first order deactivation kinetics, described by Equation 7, where  $\beta_{1,j}$  is the first order deactivation constant and  $a_j$  is the conversion at time,  $t$ , relative to the initial conversion.  $j$  denotes the type of activity: deoxygenation, hydrogenation, or C-C cleavage. The coefficient of determination ( $R^2$ ) was >0.95 for all calculated  $\beta$  values.

$$\ln(a_j) = -\beta_{1,j} t \quad (7)$$

## Acknowledgements:

This work was supported by ExxonMobil.

## References

- [1] D. Mohan, J. Charles U. Pittman, P. H. Steele, *Energy & Fuels* **2006**.
- [2] H. Yang, R. Yan, H. Chen, D. H. Lee, C. Zheng, *Fuel* **2007**, *86*, 1781-1788.
- [3] K. Routray, K. J. Barnett, G. W. Huber, *Energy Technology* **2017**, *5*, 80-93.
- [4] T. R. Carlson, Y.-T. Cheng, J. Jae, G. W. Huber, *Energy Environ. Sci.* **2011**, *4*, 145-161.
- [5] B. Donniss, R. G. Egeberg, P. Blom, K. G. Knudsen, *Topics in Catalysis* **2009**, *52*, 229-240.
- [6] A. H. Zacher, M. V. Olarte, D. M. Santosa, D. C. Elliott, S. B. Jones, *Green Chem.* **2014**, *16*, 491-515.
- [7] D. C. Elliott, T. R. Hart, G. G. Neuenschwander, L. J. Rotness, M. V. Olarte, A. H. Zacher, Y. Solantausta, *Energy & Fuels* **2012**, *26*, 3891-3896.
- [8] R. J. French, J. Stunkel, R. M. Baldwin, *Energy & Fuels* **2011**, *25*, 3266-3274.
- [9] H. Wang, J. Male, Y. Wang, *ACS Catalysis* **2013**, *3*, 1047-1070.
- [10] D. C. Elliott, *Current Opinion in Chemical Engineering* **2015**, *9*, 59-65.
- [11] D. A. Laird, R. C. Brown, J. E. Amonette, J. Lehmann, *Biofuels, bioproducts and biorefining* **2009**, *3*, 547-562.
- [12] X. Zhang, T. Wang, L. Ma, Q. Zhang, T. Jiang, *Bioresource technology* **2013**, *127*, 306-311.
- [13] R. Pindoria, A. Megaritis, A. Herod, R. Kandiyoti, *Fuel* **1998**, *77*, 1715-1726.
- [14] T. L. Marker, L. G. Felix, M. B. Linck, M. J. Roberts, *Environmental Progress & Sustainable Energy* **2012**, *31*, 191-199.
- [15] T. L. Marker, L. G. Felix, M. B. Linck, M. J. Roberts, P. Ortiz-Toral, J. Wangerow, *Environmental Progress & Sustainable Energy* **2014**, *33*, 762-768.
- [16] G. Perkins, T. Bhaskar, M. Konarova, *Renewable and Sustainable Energy Reviews* **2018**, *90*, 292-315.
- [17] T. L. Marker, G. T. I. D. P. IL, L. G. Felix, G. T. I. B. AL, M. B. Linck, G. T. I. D. P. IL, M. J. Roberts, G. T. I. D. P. IL, P. Ortiz-Toral, G. T. I. D. P. IL, J. Wangerow, G. T. I. D. P. IL, *Environmental Progress & Sustainable Energy* **2018**, *33*, 762-768.
- [18] D. C. Dayton, J. Hlebak, J. R. Carpenter, K. Wang, O. D. Mante, J. E. Peters, *Energy & Fuels* **2016**, *30*, 4879-4887.
- [19] D. C. Dayton, J. Carpenter, J. Farmer, B. Turk, R. Gupta, *Energy & Fuels* **2013**, *27*, 3778-3785.
- [20] M. Z. Stummann, M. Høj, C. B. Schandel, A. B. Hansen, P. Wiwel, J. Gabrielsen, P. A. Jensen, A. D. Jensen, *Biomass and Bioenergy* **2018**, *115*, 97-107.
- [21] M. Z. Stummann, A. B. Hansen, L. P. Hansen, B. Davidsen, S. B. Rasmussen, P. Wiwel, J. Gabrielsen, P. A. Jensen, A. D. Jensen, M. Høj, *Energy & fuels* **2019**, *33*, 1302-1313.
- [22] S. Kasiraju, L. Grabow, *AIChE Journal* **2018**.
- [23] N.-Y. Topsøe, H. Topsøe, *Journal of Catalysis* **1983**, *84*, 386-401.
- [24] T. M. H. Dabros, A. Gaur, D. G. Pintos, P. Sprenger, M. Høj, T. W. Hansen, F. Studt, J. Gabrielsen, J.-D. Grunwaldt, A. D. Jensen, *Applied Catalysis A: General* **2018**, *551*, 106-121.
- [25] H. Topsøe, B. S. Clausen, F. E. Massoth, in *Catalysis*, Springer, **1996**, pp. 1-269.
- [26] E. Laurent, B. Delmon, *Journal of Catalysis* **1994**, *146*, 281-291.
- [27] K. A. Johnson, J. B. Powell, J. A. Smegal, Google Patents, **2012**.
- [28] Q. Bu, H. Lei, A. H. Zacher, L. Wang, S. Ren, J. Liang, Y. Wei, Y. Liu, J. Tang, Q. Zhang, R. Ruan, *Bioresource Technology* **2012**, *124*, 470-477.

- [29] A. L. Jongerius, R. Jastrzebski, P. C. A. Bruijninx, B. M. Weckhuysen, *Journal of Catalysis* **2012**, *285*, 315-323.
- [30] I. D. Mora-Vergara, L. Hernández Moscoso, E. M. Gaigneaux, S. A. Giraldo, V. G. Baldovino-Medrano, *Catalysis Today* **2018**, *302*, 125-135.
- [31] A. Gutierrez, E.-M. Turpeinen, T.-R. Viljava, O. Krause, *Catalysis Today* **2017**, *285*, 125-134.
- [32] N. Chen, T. Degnan, L. Koenig, *Chemtech* **1986**, *16*, 506-511.
- [33] H. Zhang, Y.-T. Cheng, T. P. Vispute, R. Xiao, G. W. Huber, *Energy & Environmental Science* **2011**, *4*, 2297-2307.
- [34] P. J. Dietrich, R. J. Lobo-Lapidus, T. Wu, A. Sumer, M. C. Akatay, B. R. Fingland, N. Guo, J. A. Dumesic, C. L. Marshall, E. Stach, *Topics in Catalysis* **2012**, *55*, 53-69.
- [35] M. Badawi, J. Paul, S. Cristol, E. Payen, Y. Romero, F. Richard, S. Brunet, D. Lambert, X. Portier, A. Popov, *Journal of catalysis* **2011**, *282*, 155-164.
- [36] V.-L. Yfanti, A. Lemonidou, *Journal of Catalysis* **2018**, *368*, 98-111.
- [37] V. Zacharopoulou, E. S. Vasiliadou, A. A. Lemonidou, *Green Chemistry* **2015**, *17*, 903-912.
- [38] V. Zacharopoulou, E. Vasiliadou, A. A. Lemonidou, *ChemSusChem* **2017**.
- [39] V. der, D.-C. Arda Ülgen aus Istanbul Berichter, U. F. Wolfgang Hölderich Universitätsprofessor Manfred Martin, **2009**.
- [40] Y. Liu, H. Tüysüz, C.-J. Jia, M. Schwickardi, R. Rinaldi, A.-H. Lu, W. Schmidt, F. Schüth, *Chemical Communications* **2010**, *46*, 1238-1240.
- [41] G. Sánchez, J. Friggieri, C. Keast, M. Drewery, B. Dlugogorski, E. Kennedy, M. Stockenhuber, *Applied Catalysis B: Environmental* **2014**, *152*, 117-128.
- [42] C. Mésangeau, S. Yous, B. Pérès, D. Lesieur, T. Besson, *Tetrahedron letters* **2005**, *46*, 2465-2468.
- [43] E. Furimsky, F. E. Massoth, *Catalysis Today* **1999**, *52*, 381-495.
- [44] A. Stanislaus, M. Absi-Halabi, K. Al-Dolama, A. Katrib, M. Ismail, *Applied Catalysis* **1988**, *41*, 109-119.
- [45] T. M. H. Dabros, M. L. Andersen, S. B. Lindahl, T. W. Hansen, M. Høj, J. Gabrielsen, J.-D. Grunwaldt, A. D. Jensen, *Catalysts* **2019**, *9*, 521.
- [46] H. Liu, C. Yin, X. Li, Y. Chai, Y. Li, C. Liu, *Catalysis Today* **2017**, *282*, 222-229.
- [47] T. L. Marker, D. P. GTI (Gas Technology Institute), Illinois 60018, D. P. GTI (Gas Technology Institute), Illinois 60018, L. G. Felix, B. Gas Technology Institute, AL 35203-1821, M. B. Linck, D. P. GTI (Gas Technology Institute), Illinois 60018, M. J. Roberts, D. P. GTI (Gas Technology Institute), Illinois 60018, *Environmental Progress & Sustainable Energy* **2018**, *31*, 191-199.
- [48] J. T. Scanlon, D. E. Willis, *Journal of Chromatographic Science* **1985**, *23*, 333-340.

